Eur. Phys. J. C 52, 743–758 (2007)
DOI 10.1140/epjc/s10052-007-0415-3

THE EUROPEAN PHYSICAL JOURNAL C

Special Article – Scientific Note

Perspectives for the detection and measurement of supersymmetry in the focus point region of mSUGRA models with the ATLAS detector at LHC

U. De Sanctis, T. Lari, S. Montesano, C. Troncon[a]

Università di Milano – Dipartimento di Fisica and Istituto Nazionale di Fisica Nucleare – Sezione di Milano, Via Celoria 16, 20133 Milan, Italy

Received: 3 May 2007 / Revised version: 3 September 2007 /
Published online: 26 September 2007 –

Abstract. This paper discusses the potential of ATLAS to study supersymmetry in the "focus point" region of the parameter space of mSUGRA models. The potential to discover a deviation from standard model expectations with the first few fb^{-1} of LHC data was studied using the parametrized simulation of the ATLAS detector. Several signatures were considered, involving hard jets, large missing energy, and either b-tagged jets, opposite-sign isolated electron or muon pairs, or top quarks reconstructed exploiting their fully-hadronic decays. With only $1\,\mathrm{fb}^{-1}$ of data each of these signatures may allow for observing an excess of events over standard model expectations with a statistical significance exceeding five standard deviations. Furthermore, each of the two invariant mass distributions of the two leptons produced by the $\tilde{\chi}_3^0 \to \tilde{\chi}_1^0 l^+ l^-$ and the $\tilde{\chi}_2^0 \to \tilde{\chi}_1^0 l^+ l^-$ three-body decays has a kinematic endpoint that measures the difference between the masses of the parent and daughter neutralino. An analytical expression was derived for the shape of this distribution and was used to fit the simulated LHC data. A measurement of the $\tilde{\chi}_2^0 - \tilde{\chi}_1^0$ and $\tilde{\chi}_3^0 - \tilde{\chi}_1^0$ mass differences was obtained and this information was used to constrain the MSSM parameter space.

1 Introduction

One of the best motivated extensions of the standard model is the minimal supersymmetric model (MSSM) [1]. Because of the large number of free parameters of the general MSSM, the studies in preparation for the analysis of LHC data are mostly performed in a more constrained framework, obtained making some assumptions on the breaking mechanism of supersymmetry. Most studies are performed in the minimal SUGRA framework [1], which has five free parameters: the common mass m_0 of scalar particles at the grand-unification energy scale, the common fermion mass $m_{1/2}$, the common trilinear coupling A_0, the sign of the higgsino mass parameter μ and the ratio $\tan\beta$ between the vacuum expectation values of the two Higgs doublets.

Constraints are provided by searches made by experiments at accelerators (in particular LEP [2]) and by the requirements that the radiative electroweak symmetry breaking is consistent with the standard model. A strong point of supersymmetry is that in case of exact R-parity conservation the lightest SUSY particle (LSP) is stable and can thus provide a candidate for dark matter. Because of cosmological considerations the LSP must be neutral and weakly interacting and in mSUGRA the suitable candidate is the lightest neutralino $\tilde{\chi}_1^0$. It is therefore natural to apply the additional constraint that the neutralino relic density $\Omega_{\tilde{\chi}}$ in the present universe should be compatible with the density of non-baryonic dark matter, which is $\Omega_{\mathrm{DM}}h^2 = 0.105^{+0.007}_{-0.013}$ [3–5]. If there are other contributions to the dark matter one may have $\Omega_{\tilde{\chi}} < \Omega_{\mathrm{DM}}$.

In most of the mSUGRA parameter space, however, the neutralino relic density is larger than Ω_{DM} [6, 7]. An acceptable value of relic density is obtained only in particular regions of the parameter space, noticeably:

- in a region with a relatively low value of the SUSY mass scale (bulk region);
- for $m_{1/2} \gg m_0$, when the mass of the scalar τ is close to the mass of the lightest neutralino, so that $\tilde{\chi}\tilde{\tau}$ annihilation in the early universe reduces the relic density ($\tilde{\tau}$ co-annihilation region);
- for large value of $\tan\beta$, there is a funnel in the parameter space where the mass of the pseudo-scalar Higgs boson is nearly twice the one of the neutralino, enhancing the $\tilde{\chi}\tilde{\chi}$ annihilation cross section (Higgs funnel region);
- for $m_{1/2} \ll m_0$ a region exists [8–11] where the lightest neutralino has a significant higgsino component, enhancing the $\tilde{\chi}\tilde{\chi}$ annihilation cross section (focus point region).

[a] e-mail: atlas.secretariat@cern.ch

In this paper a study of the potential of ATLAS to discover and study supersymmetry in the focus point scenario is presented.

The paper is organized as follows. In Sect. 2 a scan of the minimal SUGRA parameter space is performed to map the focus point region with an acceptable relic density. The theoretical uncertainties on the SUSY mass spectrum and the variation of the masses across the focus point parameter space are discussed. Finally, a benchmark point is selected for more detailed studies. For this benchmark, the production of supersymmetric particles is dominated by the electroweak production of neutralinos and charginos, which is not easily observable in a hadronic collider, and by the pair production of gluinos, followed by the decay of each gluino into (mostly) third-generation quarks and a neutralino or chargino. The gluino pair production results in events with hard jets, including four b-jets per event, large missing energy from the lightest neutralinos that escape detection, and possibly isolated leptons from neutralino and chargino decays. These signatures are used in the studies reported in Sect. 3 to Sect. 5.

In Sect. 3 the performance of inclusive search strategies based on the presence of hard jets, large missing energy, and b-tagged jets to discriminate the SUSY signal from the standard model background is studied.

In Sect. 4 the reconstruction of the kinematic edge of the invariant mass distribution of the two leptons from the decay $\tilde{\chi}_n^0 \to \tilde{\chi}_1^0 l^+ l^-$ is discussed. The presence of isolated lepton pairs (in addition to hard jets and missing energy) is a promising discovery channel with the first few fb^{-1} of LHC data; with a larger dataset, the kinematic endpoints of the two-lepton invariant mass distribution allow for the measurement of two constraints on the masses of the three lightest neutralinos. To this aim, an analytical expression for the shape of the invariant mass distribution of the lepton pairs arising from the three-body leptonic decay of the neutralinos has been derived, in the hypothesis of heavy scalar masses (which is a suitable approximation for the focus point). The resulting function was used in the fit of the dilepton invariant mass distribution obtained with simulated data, obtaining a measurement of the $\tilde{\chi}_2^0$–$\tilde{\chi}_1^0$ and $\tilde{\chi}_3^0$–$\tilde{\chi}_1^0$ mass differences.

In Sect. 5 the reconstruction of the gluino decays is discussed. To this aim, the fully-hadronic decays of the top quark are reconstructed; the presence of an excess of tb and tt pairs is a possible discovery channel, while their invariant masses place constraints on the gluino mass scale.

Finally, Sect. 6 investigates what constraints one can put on the supersymmetry parameters from the measurements of the two neutralino mass differences.

2 Scans of mSUGRA parameter space

In order to find the regions of the mSUGRA parameter space that have a relic density compatible with cosmological measurements, the neutralino relic density was computed with micrOMEGAs 1.31 [12], interfaced with either ISAJET 7.71 [13] or SOFTSUSY 1.9 [14] for the solution of the renormalization group equations (RGE) to compute the supersymmetry mass spectrum at the weak scale.

The two spectrum calculators both consider two-loop radiative corrections in computing the running of masses and couplings between the electroweak and the unification energy scales. They differ in the implementation of these corrections, however, and the difference between their results reflects the uncertainties on the contributions from higher order radiative corrections. A detailed comparison between the RGE calculators can be found in [15], while the uncertainties on the resulting predictions of relic density are discussed in [16, 17]. Over most of parameter space, the mass spectrum is predicted with an uncertainty of less than 1%, but in the focus point region larger differences are found: in this region of parameter space the results are particularly sensitive to the value of the top Yukawa couplings and the uncertainties from higher order corrections are significant.

In Fig. 1 a scan of the $(m_0, m_{1/2})$ plane performed with ISAJET + micrOMEGAs is presented, for fixed values of $\tan\beta = 10$, $A_0 = 0$, and positive μ. A top mass of 175 GeV was used. The dark grey region on the left is the scalar tau co-annihilation strip, while that on the right is the focus point region with $\Omega_{\tilde{\chi}} < \Omega_{\rm DM}$.

The latter is found at large values of $m_0 > 3$ TeV, hence in this scenario the scalar particles are very heavy, near or beyond the sensitivity limit of LHC searches. Since $m_{1/2} \ll m_0$, the gauginos (chargino and neutralino) and gluino states are much lighter. In this scenario the SUSY production cross section at the LHC is thus dominated by gaugino and gluino pair production.

It is instructive to consider the variation of the relic density and the higgsino mass term μ along a line in the

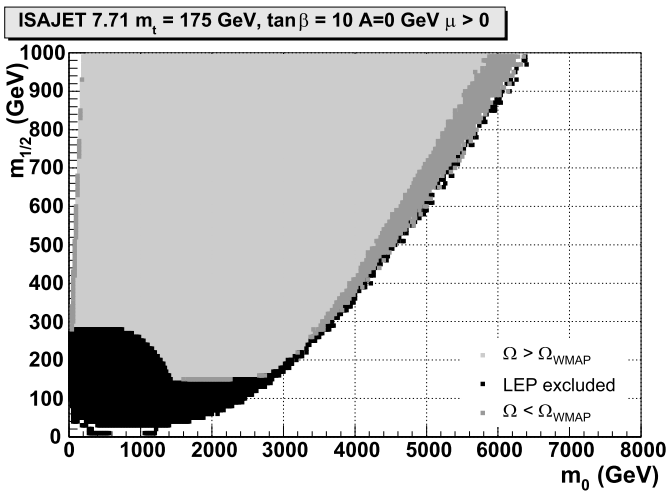

Fig. 1. The picture shows the regions of the $(m_0, m_{1/2})$ mSUGRA plane which have a neutralino relic density compatible with cosmological measurements in *dark grey*. The *black regions* are excluded by the LEP limits [2] on the mass of the lightest Higgs, chargino, and neutralino particles. The *light grey regions* have a neutralino relic density that exceeds cosmological measurements. *White regions* are theoretically excluded. The values of $\tan\beta = 10$, $A_0 = 0$, a positive μ, and a top mass of 175 GeV were used. The RGE were solved using ISAJET

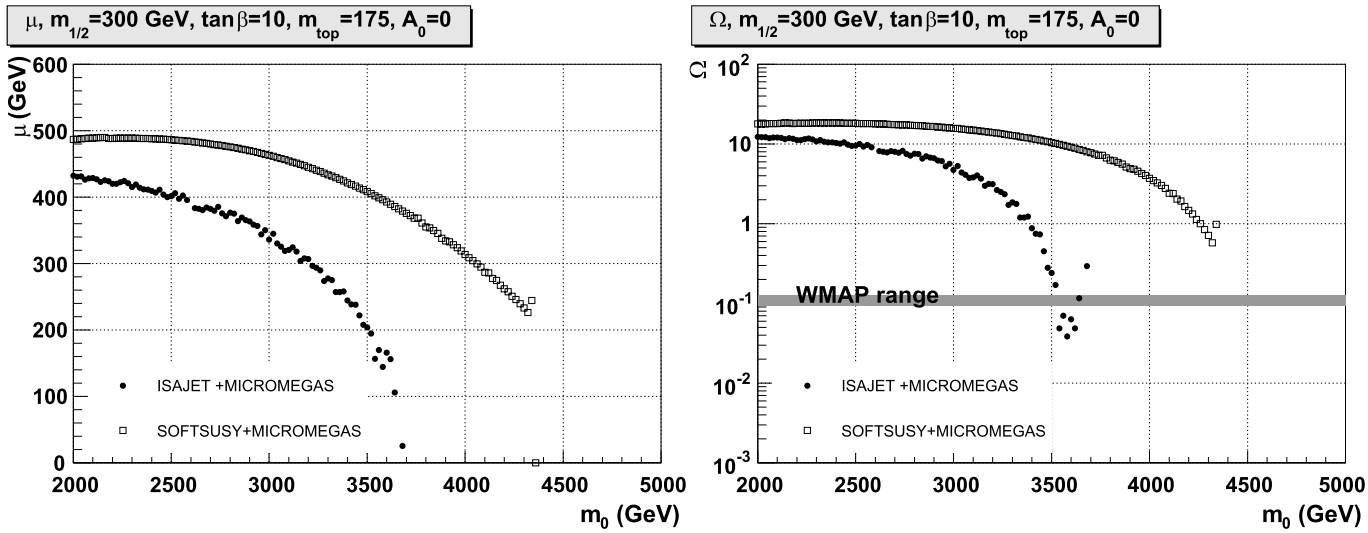

Fig. 2. *Left plot*: dependence of the higgsino mass term μ on the mSUGRA common scalar mass m_0, for $m_{1/2} = 300\,\text{GeV}$, $\tan\beta = 10$, $A_0 = 0$, a positive μ, and a top mass of 175 GeV. The *circles* are obtained using ISAJET to solve the RGEs, the *open squares* using SOFTSUSY. *Right plot*: dependence of the neutralino relic density on m_0

$(m_0, m_{1/2})$ plane at fixed $m_{1/2}$. This is shown in Fig. 2 for $m_{1/2} = 300\,\text{GeV}$. The left plot reports the dependence of μ on m_0. When the value of μ drops, the lightest neutralino acquires a significant higgsino component and the relic density decreases (as shown in the right plot): this is the focus point region. The picture shows that ISAJET and SOFTSUSY are in reasonable agreement for low values of m_0; but their predictions diverge as the scalar mass is increased, and they find the drop of μ at different values of m_0. In addition, the value computed by SOFTSUSY never gets low enough to result in an acceptable value of the relic density for this particular choice of the parameters. These uncertainties make it difficult to decide whether a given SUSY mass spectrum is really consistent with the mass and coupling unification at the high scale assumed by mSUGRA. However, this does not prevent us from selecting a benchmark point with an interesting phenomenology, compatible with accelerator and cosmological constraints, and study the ATLAS potential to study this model.

The gluino mass increases with $m_{1/2}$. It is about 800 GeV for $m_{1/2} = 300\,\text{GeV}$, at the bottom of the focus point strip allowed by cosmological constraints and accelerator searches. This value corresponds to a cross section for gluino pair production at the LHC of about 1 pb. The gluino decays to $\tilde{\chi}qq$ (a chargino or neutralino, and two quarks) followed by the cascade decays of the chargino (or neutralino) into the lightest neutralino. These events have the classical mSUGRA signature of hard jets and missing energy and can be discriminated from the standard model background as will be shown in Sect. 3.

As one moves upward inside the focus point strip, the gluino mass increases, and it reaches the value of 2 TeV for $m_{1/2} \sim 900\,\text{GeV}$. This is expected to be roughly the limit of the discovery potential of ATLAS [18]. The masses of the lightest neutralino and chargino states are much smaller than the gluino and squark masses, and the cross section for $\tilde{\chi}\tilde{\chi}$ production at the LHC can be larger than the cross section for gluino pair production. Since the gauginos are very light, however, their decay does not provide a signature with hard jets and missing energy, which would allow for discrimination against the standard model background. The possibility to detect this signal through multilepton signatures is under study, and it is outside the scope of this note.

No focus point solution is found for $\tan\beta < 7$. For large values of $\tan\beta$, the focus point solutions move to lower values of m_0 as shown in Fig. 3. For a fixed value of $m_{1/2}$, the gluino and gaugino masses are hardly affected. However, the masses of the scalars become smaller, and the production of $\tilde{q}\tilde{g}$ and $\tilde{q}\tilde{q}$ pairs, followed by the squark cascade decay into gluinos, chargino and neutralinos, may be observed at LHC. Note also that the width of the coannihilation strip is heavily affected by the value of $\tan\beta$.

The position of the focus point strip is also very sensitive to the value of the top mass. A lighter top pushes the focus point strip to smaller values of m_0 (Fig. 4). The relation between the value of the scalar mass m_0 for which a focus point solution is found and the top mass is shown in Fig. 5 for fixed values of $\tan\beta = 10$, $A = 0$, $\mu > 0$ and $m_{1/2} = 300\,\text{GeV}$.

The location of the focus point strip in the $(m_0, m_{1/2})$ is much less sensitive to the choice of the sign of μ or the value of A, at least in the range between $-1000\,\text{GeV}$ and 1000 GeV.

From the considerations above the following point in the parameter space was chosen for the detailed study reported in the next sections:

$$m_0 = 3550\,\text{GeV}, \quad m_{1/2} = 300\,\text{GeV}, \quad A = 0\,\text{GeV}, \\ \mu > 0, \quad \tan\beta = 10\,,$$

with the top mass set to 175 GeV and the mass spectrum computed with ISAJET. In Table 1 the mass spec-

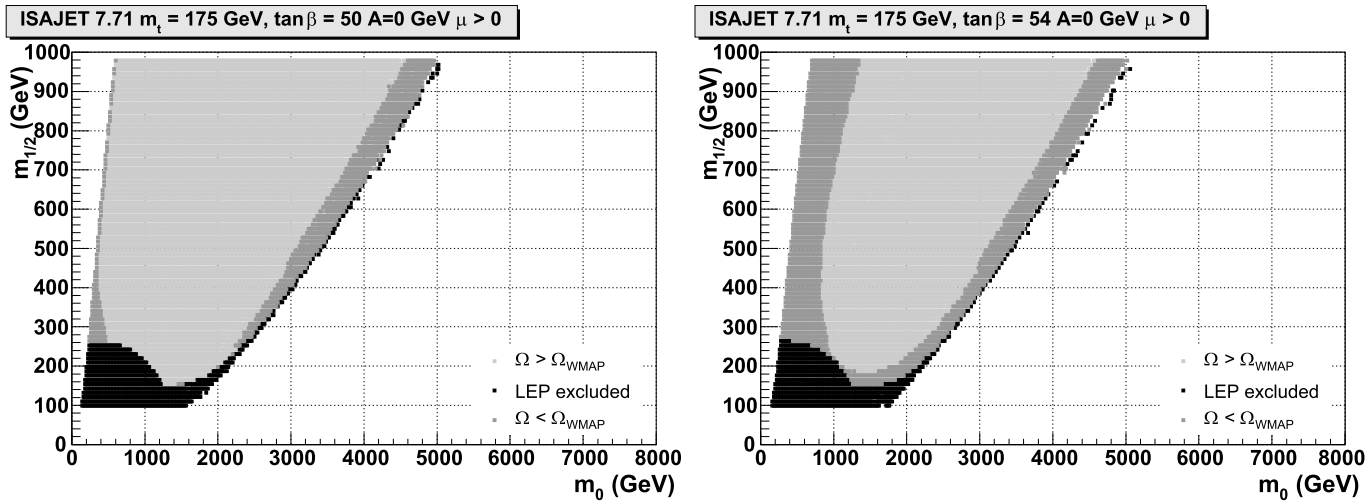

Fig. 3. Same as Fig. 1, but for $\tan\beta = 50$ (*left plot*) and $\tan\beta = 54$ (*right plot*)

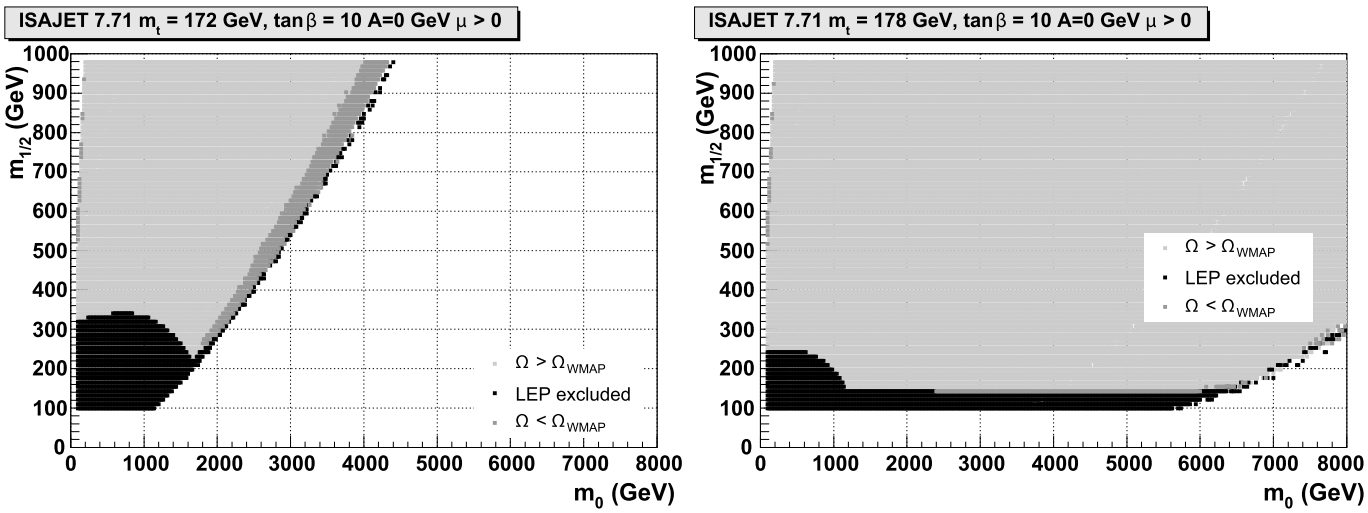

Fig. 4. Same as Fig. 1, but for a top mass of 172 GeV (*left plot*) and 178 GeV (*right plot*)

trum for this point is given. The scalar partners of standard model fermions have a mass between 2131 GeV and 3574 GeV. The neutralinos and charginos have masses between 103.3 GeV and 294.9 GeV. The gluino is the lightest strongly interacting state, with a mass of 856.6 GeV. The lightest Higgs boson has a mass of 119 GeV, while the other Higgs states have masses at more than 3 TeV, well beyond the expected reach of LHC.

At this point of the mSUGRA parameter space, the total SUSY production cross section at the LHC, as computed by HERWIG [20–22] at leading order, is 5.00 pb. It is dominated by the production of gaugino pairs, $\tilde{\chi}^0\tilde{\chi}^0$ (0.22 pb), $\tilde{\chi}^0\tilde{\chi}^\pm$ (3.06 pb), and $\tilde{\chi}^\pm\tilde{\chi}^\pm$ (1.14 pb).

The production of gluino pairs (0.58 pb) is also significant. The gluino decays into $\tilde{\chi}^0 q\bar{q}$ (29.3%), $\tilde{\chi}^0 g$ (6.4%), or $\tilde{\chi}^\pm q\bar{q}'$ (54.3%). The quarks in the final state belong to the third generation in 75.6% of the decays.

The more recent Tevatron data favor a lighter top mass [19]. As the location of the focus point region in parameter space is quite sensitive to the value of the top mass, it is opportune to discuss how the phenomenology of our benchmark would change by using a lower value of 172 GeV for the top mass. The correct relic density can be obtained lowering the value of m_0 to 2000 GeV. The gluino would then have a slightly lower mass of 818 GeV. The neutralino and chargino masses are also slightly smaller, but they remain within 10 GeV of the values of those of our benchmark point. The leptonic decays of the $\tilde{\chi}_2^0$ and $\tilde{\chi}_3^0$, which are the basis of the analysis discussed in Sect. 4, still occur, but with a smaller branching ratios (1.9% and 3.3% instead of 3.3% and 3.8%).

In this scenario, the event rates would be slightly different from rates in our benchmark scenario, but the procedures and the general conclusions of the studies presented in the next sections would still hold.

In addition, the lower value of m_0 would probably open up the possibility to discover the scalar quarks at the LHC.

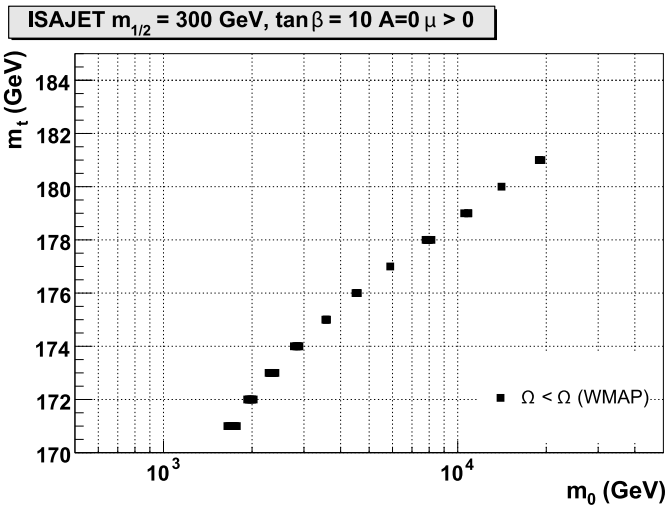

Fig. 5. The picture shows the values of the mSUGRA common scalar mass m_0 and the top mass m_t that have a neutralino relic density compatible with cosmological measurements. The values of $m_{1/2} = 300$ GeV, $\tan\beta = 10$, $A_0 = 0$, and a positive μ were used. The RGE were solved using ISAJET

Table 1. The mass spectrum of the benchmark focus point described in the text

Particle	Mass (GeV)	Particle	Mass (GeV)
$\tilde{\chi}_1^0$	103.35	$\tilde{e}_{\mathrm{L}}$	3547.5
$\tilde{\chi}_2^0$	160.37	$\tilde{e}_{\mathrm{R}}$	3547.5
$\tilde{\chi}_3^0$	179.76	$\tilde{\nu}_e$	3546.3
$\tilde{\chi}_4^0$	294.90	$\tilde{\tau}_1$	3519.6
$\tilde{\chi}_1^\pm$	149.42	$\tilde{\tau}_2$	3533.7
$\tilde{\chi}_2^\pm$	286.81	$\tilde{\nu}_\tau$	3532.3
$\tilde{g}$	856.59	h	119.01
$\tilde{u}_{\mathrm{L}}$	3563.2	H^0	3529.7
$\tilde{u}_{\mathrm{R}}$	3574.2	A^0	3506.6
$\tilde{b}_1$	2924.8	$H^\pm$	3530.6
$\tilde{b}_2$	3500.6		
$\tilde{t}_1$	2131.1		
$\tilde{t}_2$	2935.4		

3 Inclusive searches

In this section, the possibility to detect an excess over standard model expectations in the production of events with hard jets and large missing energy is investigated. The cuts will be optimized to be sensitive to the production of gluino pairs, but they will not rely on any specific decay of the gluino or its daughters.

The production of supersymmetry events at the LHC was simulated using HERWIG 6.55 [20–22]. The top background was produced using MC@NLO 2.31 [23, 24]. The fully inclusive $t\bar{t}$ production was simulated. This is expected to be the dominant standard model background for the analysis presented here.

The $Z+$jets and the $W+$jets backgrounds were produced with ALPGEN 2.05 [25–27] for the hard process, requiring at least 2 jets with $p_{\mathrm{T}} > 40$ GeV, $|\eta| < 6$, and an angular separation in the plane of pseudorapidity and azimuthal angle of at least $\Delta R = \sqrt{\Delta\eta^2 + \Delta\phi^2} > 0.7$. HERWIG was used for the subsequent parton shower and hadronization. Only the W leptonic decays and the Z decays into charged leptons or neutrinos were considered. The matrix element for $W+$jets and $Z+$jets used by ALPGEN only includes the associated production of the boson with light (first two generation) quarks and gluons; however, $b\bar{b}$ pairs are produced by gluon splitting during the parton shower. The $Z \to b\bar{b}$ decays are not included, because we are interested in processes that give a large missing energy. The process $Z \to b\bar{b}$ has a branching ratio comparable to $Z \to \nu\bar{\nu}$ and a much smaller missing transverse energy, so it is not expected to give a significant contribution to the background of the analysis documented here.

The $b\bar{b}+$jets background[1] was simulated using ALPGEN for the hard process, requiring $|\eta| < 5$ and $p_{\mathrm{T}} > 40$ GeV for the b quarks and $|\eta| < 3$ and $p_{\mathrm{T}} > 40$ GeV for the additional jets (at least one). HERWIG was used for the simulation of the subsequent parton shower and hadronization. The QCD light jet background is expected to be negligible for the analysis presented here, which requires either two tagged b-jets or isolated leptons. In order to verify this assumption, the production of events with three or more jets with $p_{\mathrm{T}} > 40$ GeV was simulated using ALPGEN for the hard process and HERWIG for parton shower and hadronization. All jet flavours except b-jets were included.

The events were then processed by ATLFAST [28] to simulate the detector response.

A list of the simulated data used for fast simulation studies is shown in Table 2. The different instantaneous luminosities are taken into account through the parametrization used by ATLFAST to simulate the detector response, since during operation at low luminosity ($10^{33}\,\mathrm{cm}^{-2}\mathrm{s}^{-1}$) the detector performance is not degraded by pile-up effects. The standard parametrization of the ATLAS b-tagging performance was used, which assumed a b-tagging efficiency of 0.6 at low luminosity and 0.5 at high luminosity, for a rejection factor (the inverse of efficiency) for charm and light quark jets of 10 and 100 respectively. Muons and electrons are considered isolated if they are separated by the closest calorimeter cluster in the plane of pseudorapidity and azimuthal angle by at least $\Delta R = \sqrt{\Delta\eta^2 + \Delta\phi^2} > 0.4$ and if the transverse energy measured by the calorimeter in a cone centered on the lepton and of width $\Delta R = 0.2$ is not larger than 10 GeV (excluding the energy of the lepton itself).

Trigger efficiencies were not taken into account by the detector simulation. The cuts of the analyses described in this and in the following sections are more stringent than the selections of the ATLAS trigger menu foreseen for operation at the design luminosity of LHC [29]. In particular, the cuts on jets and missing energy are more severe than the trigger requirement of at least one jet with $p_{\mathrm{t}} > 70$ GeV

[1] This includes only the QCD production, and not the electroweak process $Z(b\bar{b})+$jets, discussed above.

Table 2. Simulated data samples used for the fast simulation studies reported here. The first two columns report the process simulated and the event generator software used. The third column reports the inclusive cross section of the process; the fourth column reports the cross section after the generator-level cuts described in the text. The next two columns report the number of events simulated and the corresponding integrated luminosity. The last column reports the instantaneous luminosity assumed for the simulation of pile up effects on the detector reconstruction

Process	Generator	σ (pb)	σ_2 (pb)	Events (10^6)	$\int L\mathrm{d}t$ (fb^{-1})	L (cm^{-2}s^{-1})
SUSY	HERWIG	5.0	5.0	0.15	30	10^{33}
SUSY	HERWIG	5.0	5.0	1.5	300	10^{34}
$t\bar{t}$	MC@NLO	760	760	16.7	22	10^{33}
W+jets	ALPGEN	51 420	1010	18.2	18	10^{33}
Z+jets	ALPGEN	8710	315	6.3	20	10^{33}
$bb+N$ jets ($N=1$)	ALPGEN	$\sim 10^9$	22 440	10.9	0.49	10^{33}
$bb+N$ jets ($N>1$)	ALPGEN	$\sim 10^9$	4900	11.6	2.4	10^{33}
N jets ($N=3$)	ALPGEN	$\sim 10^{11}$	999 000	6.69	0.0067	10^{33}
N jets ($N>3$)	ALPGEN	$\sim 10^{11}$	122 200	1.15	0.0096	10^{33}

and $E^{\mathrm{T}}_{\mathrm{Miss}} > 70$ GeV. Many of the events used in the analysis presented in the next section, with two isolated leptons in the final state, would also be selected by the electron and muon triggers. A study of the impact of trigger efficiencies on event rates, as well as the inclusions of detector effects not described by the parametrized simulation is outside the scope of this document.

We now consider the number of events of the QCD multi-jet background that pass an event selection that is looser than the cuts required by all the analysis discussed in this paper. Our purpose is to show that most of this background comes from the $bb+$jets process, and that the production from the production of light quarks can be neglected.

Our loose selection requires at least 70 GeV of missing transverse energy, at least four jets with $p_{\mathrm{T}} > 40$ GeV, and either two b-jets of $p_{\mathrm{T}} > 30$ GeV or at least one isolated lepton with $p_{\mathrm{T}} > 5$ GeV.

The results reported in Table 3 demonstrate that after this selection most of the QCD multi-jet background comes from $b\bar{b}+$jets; in the rest of the paper the QCD light jet background will not be considered.[2]

The most abundant gluino decay modes are $\tilde{g} \to \tilde{\chi}^0 t\bar{t}$ (27.9%), $\tilde{g} \to \tilde{\chi}^+ t\bar{b}$ (22.0%) and $\tilde{g} \to \tilde{\chi}^- \bar{t}b$ (22.0%).[3] Events with gluino pair production have thus at least four hard jets and may have many more additional jets because of the top hadronic decay modes and the chargino and neutralino hadronic decay modes, such as $\tilde{\chi}^0_2 \to \tilde{\chi}^0_1 q\bar{q}$ or $\tilde{\chi}^\pm_1 \to \tilde{\chi}^0_1 q\bar{q}'$. When both gluinos decay to third-generation quarks, which happens for 57.2% of the events, at least 4 jets are b-jets. A missing energy signature is provided by the two $\tilde{\chi}^0_1$ in the final state, and possibly by neutrinos coming from the top quark and the gaugino leptonic decay modes.

[2] Studies based on a detailed detector simulation [18] show that the probability to misidentify a jet as an isolated lepton is of the order of 10^{-5}. Such a misidentification rate would not significantly affect the results reported in Table 3.

[3] In the following, whenever the decay $\tilde{g} \to t\bar{b}\tilde{\chi}^-$ will be mentioned, the charge conjugate is implied.

Table 3. Contributions of the multi jet background to the signatures studied in this paper, evaluated with ATLFAST events for low luminosity operation. The number of events corresponds to an integrated luminosity of 9.6 pb^{-1}; the second column reports the number of events in the simulated data sample after generator-level preselections. The third column shows the number of events which have $E^{\mathrm{T}}_{\mathrm{Miss}} > 70$ GeV and four jets with $p_{\mathrm{T}} > 40$ GeV. The fourth column reports the number of events after the additional requirement of two tagged b-jets with $p_{\mathrm{T}} > 30$ GeV. The last column reports the number of events after the selections of the third column plus at least one isolated electron or muon with $p_{\mathrm{T}} > 5$ GeV

Process	Events	$E^{\mathrm{T}}_{\mathrm{Miss}}$ and 4 jets cut	2 b-jets	1 lepton
$bb+$jets	263 800	357	106.1	5.2
light jets	1.08×10^7	1072	4.1	1.0

These events can be separated from the standard model background requiring the presence of hard jets and a large missing transverse energy. The request of b-jets in the final state suppresses the $W+$jets and $Z+$jets background so that the dominant surviving standard model background is the top pair production and the $bb+$jets production. This request also enhances the signal with respect to these backgrounds, as most signal events have four true b-jets (rather than two) in the final state.

The following selections are made:

- at least one jet with $p_{\mathrm{T}} > 120$ GeV;
- at least four jets with $p_{\mathrm{T}} > 50$ GeV, and at least two of them tagged as b-jets;
- $E^{\mathrm{T}}_{\mathrm{MISS}} > 100$ GeV;
- $E^{\mathrm{T}}_{\mathrm{MISS}}/M_{\mathrm{EFF}} > 0.12$.

Here, the effective mass M_{EFF} is defined as the scalar sum of the transverse missing energy and the transverse momentum of all the reconstructed hadronic jets. The fraction $s = E^{\mathrm{T}}_{\mathrm{MISS}}/M_{\mathrm{EFF}}$ measures the relative importance of the missing energy and the hadronic jet components of M_{EFF}. In events due to the production of a gluino pair this ratio is on average larger than in the background processes.

The efficiency of these cuts is reported in Table 4. The SUSY events are divided in gluino pair and gaugino pair production. The selection efficiency for the $\tilde{g}\tilde{g}$ events is 60.7% after all the cuts except the request of two b-tagged jets. This request reduces the selection efficiency to 28.0%. The ratio between the number of $\tilde{\chi}\tilde{\chi}$ and $\tilde{g}\tilde{g}$ events is already suppressed by two orders of magnitude by the selections on hard jets and missing energy, and it becomes negligible after the request of two b-jets.

The requirement of two b-jets dramatically reduces the $W+$jets and $Z+$jets backgrounds. Because of the large number of true b-jets in the SUSY events, it also reduces the signal less than the $t\bar{t}$ and $b\bar{b}$ backgrounds. These are the dominant sources of standard model backgrounds after all selections.

The distribution of the effective mass after these selection cuts is reported in Fig. 6. The statistics corresponds to an integrated luminosity of $10\,\mathrm{fb}^{-1}$. The number of signal and background events with an effective mass larger than 1600 GeV is comparable and is reported in the last column of Table 4.

From these numbers, it is possible for the focus point scenario under study to estimate the minimum integrated luminosity required to observe a deviation from standard model expectations. The statistical significance of the signal from supersymmetry is $S/\sqrt{B} = 6.1$ for an integrated luminosity of $1\,\mathrm{fb}^{-1}$. These numbers assume nominal detector performances (that is, detector commissioning has been completed) and includes only the statistical error on the background, which is $\sigma_{\mathrm{stat}}(B)/B = \sqrt{B}/B = 12\%$ for $1\,\mathrm{fb}^{-1}$ of integrated luminosity. A study of the various sources of systematic uncertainties and their possible evolution with integrated luminosity is beyond the scope of this study.

Table 4. Efficiency of the cuts used for the inclusive search, evaluated with ATLFAST events for low luminosity operation. The number of events corresponds to an integrated luminosity of $10\,\mathrm{fb}^{-1}$. The third column shows the number of events that pass the cuts of at least one jet with $p_{\mathrm{T}} > 120$ GeV, at least four jets with $p_{\mathrm{T}} > 50$ GeV, transverse missing energy larger than 100 GeV, and $E^{\mathrm{T}}_{\mathrm{MISS}}/M_{\mathrm{EFF}} > 0.12$. The number of events shown in the fourth column is obtained after the additional requirement that two of the jets are tagged as b-jets. Finally, the number of events which passes all the selections and have an effective mass larger than 1600 GeV is shown in the last column

Sample	Events	Basic cuts	2 b-jets	$M_{\mathrm{eff}} > 1600$ GeV
SUSY ($\tilde{\chi}\tilde{\chi}$)	44 200	359	20	0
SUSY ($\tilde{g}\tilde{g}$)	5800	3522	1625	508
$t\bar{t}$	7.6×10^6	174 993	39 816	506
W+jets	10.1×10^6	62 546	397	18
Z+jets	3.15×10^6	45 061	306	20
bb+jets	272×10^6	39 579	12124	141

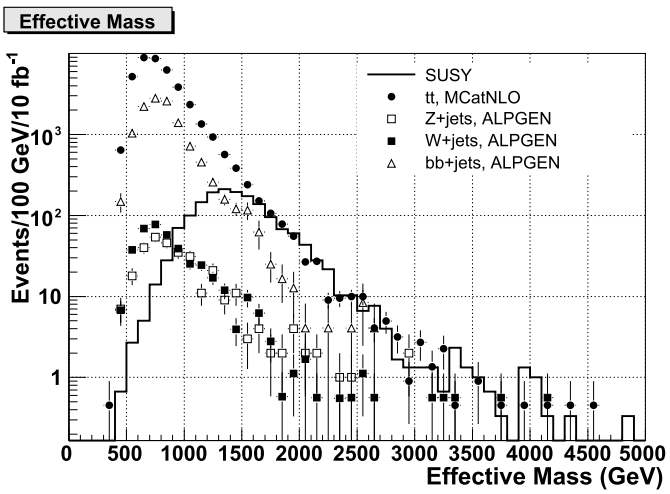

Fig. 6. Distribution of the effective mass defined in the text, for SUSY events and the standard model background, for an integrated luminosity of $10\,\mathrm{fb}^{-1}$

4 The dilepton edge

As discussed at the end of Sect. 2, at the selected benchmark point the neutralinos are produced either directly or by gluino decays. Despite the lower cross section, the latter mechanism dominates after the cuts on missing energy and jets, which are necessary to remove the standard model backgrounds. The leptonic decays of the second and third neutralino,

$$\tilde{\chi}^0_2 \to \tilde{\chi}^0_1 l^+ l^- \,, \quad (1)$$

$$\tilde{\chi}^0_3 \to \tilde{\chi}^0_1 l^+ l^- \quad (2)$$

occur with a branching ratio of 3.3% and 3.8% per lepton flavour respectively. The two leptons in the final state provide a clear signature. Their invariant mass distribution has a kinematic endpoint value equal to the mass difference of the two neutralinos involved in the decay, which is

$$m_{\tilde{\chi}^0_2} - m_{\tilde{\chi}^0_1} = 57.02\,\mathrm{GeV}\,, \quad m_{\tilde{\chi}^0_3} - m_{\tilde{\chi}^0_1} = 76.41\,\mathrm{GeV}\,. \quad (3)$$

The fourth neutralino is heavy enough that the decay $\tilde{\chi}^0_4 \to \tilde{\chi}^0_1 Z^0$ is open; the leptons produced by this decay have an invariant mass equal to the Z mass and do not allow one to measure the neutralino masses.

The leptonic decays of χ^0_2 and χ^0_3 proceed according to the two diagrams reported in Fig. 7. The resulting distribution of the lepton four momenta is given in [30].

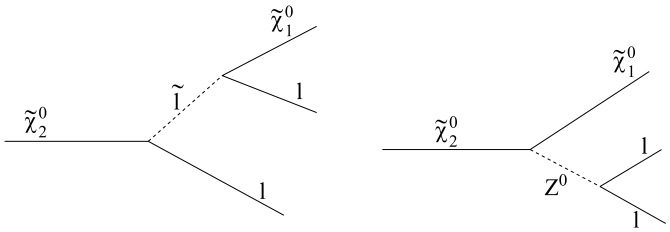

Fig. 7. Feynman diagrams of the $\tilde{\chi}^0_2$ leptonic decay. The decay of the $\tilde{\chi}^0_3$ proceeds according to a similar diagram

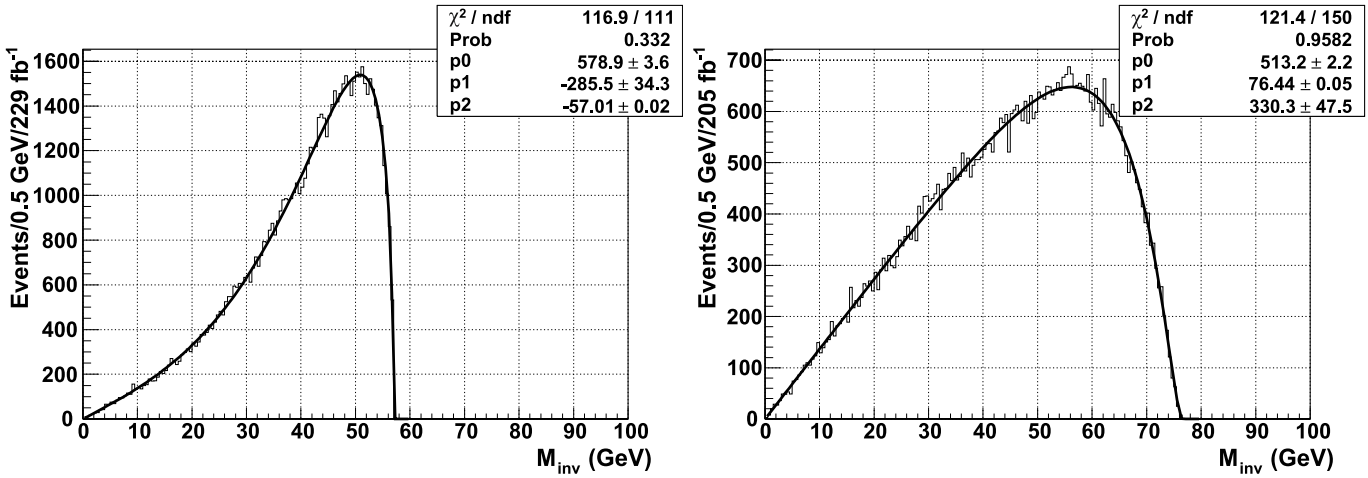

Fig. 8. Distribution of the invariant mass of lepton pairs from the $\tilde{\chi}_2^0 \to \tilde{\chi}_1^0 ll$ decay (*left plot*) and the $\tilde{\chi}_3^0 \to \tilde{\chi}_1^0 ll$ decay (*right plot*). The histogram is the HERWIG Monte Carlo distribution, the line is a fit performed with the analytical formula described in the text

In the focus point region, the diagram with the virtual slepton exchange is negligible, because of the large slepton mass. Assuming that only the diagram with the Z exchange contributes, and neglecting the masses of the leptons in the final state, we get the following expression [31] for the distribution of the two-lepton invariant mass:

$$\frac{\mathrm{d}\Gamma}{\mathrm{d}m} = Cm\frac{\sqrt{m^4 - m^2\left(\mu^2+M^2\right)+(\mu M)^2}}{\left(m^2-m_Z^2\right)^2} \times \left[-2m^4+m^2(2M^2+\mu^2)+(\mu M)^2\right]. \quad (4)$$

In this formula, C is a normalization constant, $\mu = m_2 - m_1$ and $M = m_2 + m_1$, where m_1 and m_2 are the signed mass eigenvalues of the daughter and parent neutralino respectively. At the focus point, the mass eigenvalues of the two lightest neutralinos have the same sign, while $\tilde{\chi}_0^3$ has the opposite sign. In the decay of the $\tilde{\chi}_0^2$ it is thus $\mu = m(\tilde{\chi}_2^0) - m(\tilde{\chi}_1^0)$ and $M = m(\tilde{\chi}_2^0) + m(\tilde{\chi}_1^0)$. In the decay of the $\tilde{\chi}_0^3$ the role of μ and M is inverted.[4]

The shape of the distribution is different in the two cases, as can be seen from Fig. 8, where the distribution of the invariant mass of the two leptons from the two decays is shown. The histogram is the true invariant mass of the two leptons and the line is a fit performed with the function of (4).

The fit provides both the difference and the sum of the neutralino masses. The latter is however much less precise, since the dependence of the distribution shape on the lightest neutralino mass becomes very weak when this mass is larger than the difference between the masses of the neutralinos. The results of the fit to the Monte Carlo distribution are in agreement with the true values of the neutralino masses, with the exception of the $m(\tilde{\chi}_2^0) - m(\tilde{\chi}_1^0)$ mass difference, which is precise enough to be affected by the mass of the muon, which is neglected in (4). The formula neglects the distortion of the shape caused by the kinematical cuts. The systematic errors on the mass difference arising from the analysis cuts on the lepton transverse momentum and pseudorapidity have been estimated as follows. When the kinematical cuts of the analysis on the lepton momenta ($p_{\mathrm{T}} > 10\,\mathrm{GeV}$ and $|\eta| < 2.5$) are imposed, the value of the endpoints obtained from the fit of the Monte Carlo truth distribution changes by 0.20 GeV for the $m(\tilde{\chi}_2^0) - m(\tilde{\chi}_1^0)$ difference and by 0.04 GeV for the $m(\tilde{\chi}_3^0) - m(\tilde{\chi}_1^0)$ difference. This was taken as the systematic error induced on the endpoint by the kinematical cuts.

The analysis of the simulated data was performed with the following selections:[5]

- two isolated leptons with opposite charge and same flavour with $p_{\mathrm{T}} > 10\,\mathrm{GeV}$ and $|\eta| < 2.5$;
- $E_{\mathrm{MISS}}^{\mathrm{T}} > 80\,\mathrm{GeV}$, $M_{\mathrm{EFF}} > 1200\,\mathrm{GeV}$ and $E_{\mathrm{MISS}}^{\mathrm{T}}/M_{\mathrm{EFF}} > 0.06$;
- at least one jet with $p_{\mathrm{T}} > 80\,\mathrm{GeV}$, at least four jets with $p_{\mathrm{T}} > 60\,\mathrm{GeV}$, and at least six jets with $p_{\mathrm{T}} > 40\,\mathrm{GeV}$.

The efficiency of the various cuts is shown in Table 5 for low-luminosity running conditions and integrated statistics of $30\,\mathrm{fb}^{-1}$. After all cuts, 411 SUSY and 83 standard model events are left with a two-lepton invariant mass smaller than 80 GeV. In 247 of the SUSY events the decay (1) or (2) is indeed present in the Monte Carlo Truth record. In Fig. 9 the distribution of the invariant

[4] The second term in parentheses in (4), $m^2(2M^2+\mu^2)$, is not invariant under the exchange of μ and M. This term comes from an interference term in the matrix element of the decay and does depend on the relative sign of the two neutralino eigenstates.

[5] The requirements over the leading jet p_{T} and missing energy are softer than an in inclusive analysis, since the requirement of two isolated leptons already suppresses the standard model background. The dominant background is still $t\bar{t}$, but it is dominated by events with both tops decaying leptonically, which have a relatively smaller number of jets; this leads to the cut on the sixth jet p_{T}.

Table 5. Efficiency of the cuts used for the reconstruction of the neutralino leptonic decay, evaluated with ATLFAST events for low luminosity operation. The number of events corresponds to an integrated luminosity of 30 fb^{-1}. The third column contains the number of events after all cuts, and the last column reports the number of events with a lepton invariant mass in the signal region. SUSY events are divided in gluino pair production with the presence of either the $\tilde{\chi}_2^0 \to \tilde{\chi}_1^0 l^+ l^-$ or the $\tilde{\chi}_3^0 \to \tilde{\chi}_1^0 l^+ l^-$ decay (signal), gluino pair production without these decays (background), and the $\tilde{\chi}\tilde{\chi}$ production

Sample	Events	after cuts	$M_{ll} < 80$ GeV
$\tilde{g}\tilde{g}$ signal	1027	259	247
$\tilde{g}\tilde{g}$ background	16 490	358	159
$\tilde{\chi}\tilde{\chi}$	132 483	7	5
$t\bar{t}$	22.7×10^6	131	77
W+jets	30.3×10^6	0	–
Z+jets	9.45×10^6	18	6
bb+jets	817×10^6	12	0

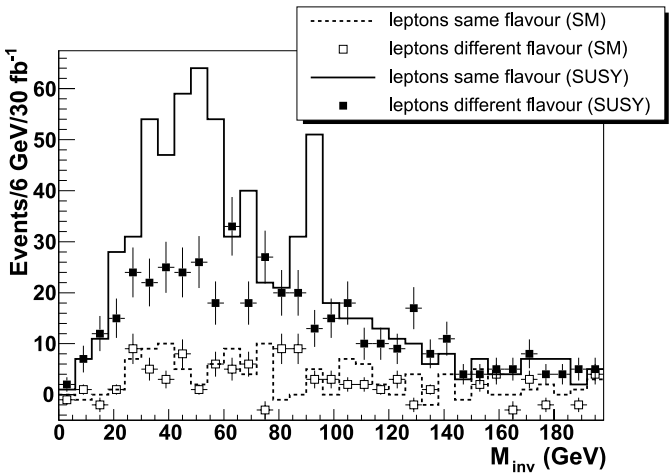

Fig. 9. The *full* and *dashed lines* are the distribution of the invariant mass of lepton pairs with the same fl avor and opposite charge for SUSY events and the standard model background respectively. The full markers (supersymmetry) and the empty markers (standard model) are the distribution of the invariant mass of the lepton pairs with opposite fl avor and opposite charge. The number of events corresponds to an integrated luminosity of 30 fb^{-1}

mass of lepton pairs after all cuts is shown for the signal and the standard model background (full and dashed lines respectively).

With these selections, the significance SUSY/$\sqrt{\text{SM}}$ would be 8.2 with an integrated luminosity of 1 fb^{-1} (neglecting systematic errors), which makes this channel competitive with the inclusive search in terms of the discovery reach.

The background can be estimated from the data using the $e^+\mu^-$ and μ^+e^- pairs. In Fig. 9 the distribution of the invariant mass of the lepton is reported for the same flavour and the opposite-flavour lepton pairs. Outside the signal region and the Z peak the two histograms are compatible. The opposite-flavour distribution was thus used to estimate and subtract the SUSY combinatorial and standard model backgrounds from the same-flavour signal histogram.

We note that this technique may be used also in the search for a deviation from standard model predictions. Since part of the SUSY events is removed in the subtraction, the statistical significance would be smaller than that obtained with the number of events with opposite-sign, same-flavour leptons. However, the standard model contribution is canceled in the subtraction, removing many sources of systematics errors on the background rates.

After the flavour subtraction and for statistics of 30 fb^{-1}, 179 ± 32 SUSY events and 19 ± 37 standard model events are left.[6] If the invariant mass of the lepton pair is required to be smaller than 80 GeV, this leaves 170 ± 25 SUSY events and 8 ± 13 standard model events. The significance of the signal from neutralino leptonic decays is 2.5 for 1 fb^{-1} of integrated luminosity.

After the flavour subtraction, the standard model background is compatible with 0 but still contributes to the invariant mass distribution by increasing the statistical fluctuations. The effect is small, since even before flavour subtraction the standard model contribution is smaller than the SUSY combinatorial background. For the high-luminosity studies reported in the rest of this section, the standard model contribution is not included.

The flavour subtracted distribution is shown in Fig. 10 for an integrated luminosity of 300 fb^{-1} and high-luminosity conditions (including pile-up effects). The presence of two edges is now apparent. The fit was performed with the sum of the $\tilde{\chi}_3^0$ and $\tilde{\chi}_2^0$ decay distributions provided by (4), convoluted with a Gaussian smearing obtained from the width of the observed Z peak. The fit parameters are the mass of the $\tilde{\chi}_1^0$ (which is the same for the two decays), the two $\tilde{\chi}_2^0$–$\tilde{\chi}_1^0$ and $\tilde{\chi}_3^0$–$\tilde{\chi}_1^0$ mass differences, and the normalizations of the two decays. A good fit χ^2 is only obtained using the correct values for the sign of the neutralino mass eigenstates.

The values found for the two mass differences are $m(\tilde{\chi}_2^0) - m(\tilde{\chi}_1^0) = (57.2 \pm 0.4 \pm 0.2)$ GeV and $m(\tilde{\chi}_3^0) - m(\tilde{\chi}_1^0) = (78.1 \pm 1.4 \pm 0.04)$ GeV. The first error is the statistical one and the second one is the systematic error due to the distortion of the distribution arising from the lepton kinematics cuts discussed earlier. They are compatible with the true values (3). The mass of the lightest neutralino is not constrained by the fit, which gives $m(\tilde{\chi}_1^0) = (0.3 \pm 2.1)$ TeV.

[6] The quoted error is the uncertainty on the Monte Carlo prediction, and it is not equal to the square root of the number of events. The expected number of events is computed as $b \times ((N_{\text{SF}+} - N_{\text{SF}-}) - (N_{\text{OF}+} - N_{\text{OF}-}))$, where b is the factor needed to rescale the Monte Carlo statistics to 30 fb^{-1}, $N_{\text{SF}+}$ and $N_{\text{SF}-}$ are the number of same-flavour events with positive weight and negative weight respectively, and $N_{\text{SF}+}$ and $N_{\text{SF}-}$ are the corresponding numbers for opposite-flavour events. The error on this number is $b \times \sqrt{N_{\text{SF}+} + N_{\text{SF}-} + N_{\text{OF}+} + N_{\text{OF}-}}$. For the SUSY sample all events have positive weight and $b = 1$, while for the top sample $b = 1.36$ and events with both positive and negative weights are present.

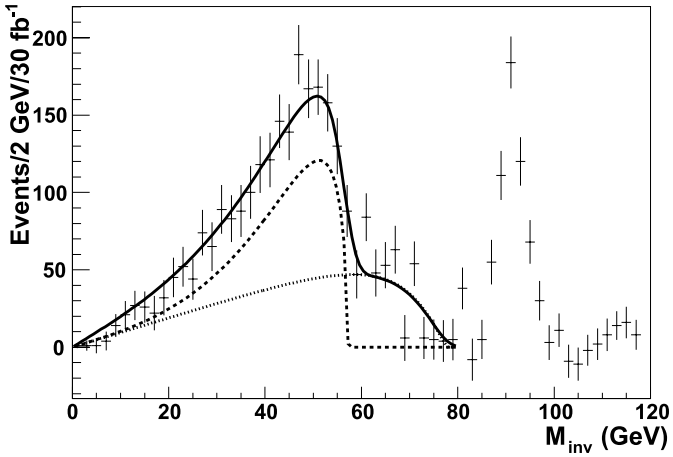

Fig. 10. Fl avor-subtracted distribution of the invariant mass of lepton pairs, for an integrated luminosity of 300 fb^{-1}. The fit function is superimposed as a *full line*; the contribution from the $\tilde{\chi}_2^0$ and $\tilde{\chi}_3^0$ decays are shown separately as a *dashed* and *dotted line* respectively

The number of events due to each neutralino decay can be computed as the integral of (4). The ratio of the events produced by the two decays can thus be determined from the parameters measured by the fit. Taking into account the correlation between the parameters, this gives $N_3/N_2 = 1.4 \pm 0.3$. This is compatible from the value $N_3/N_2 = 1.19$, which can be computed from the gluino, chargino and neutralino branching ratios.

5 Reconstruction of the gluino decays

The standard technique used to reconstruct the squark and gluino decays in mSUGRA is the combination of the leptons from the neutralino decays with the hardest jets in the event [18, 33, 34]. In models for which the two hardest jets in the event correspond to the quarks from the $\tilde{q} \to q\tilde{\chi}^0$ decay, it is possible to control the combinatorics from wrong jet associations and reconstruct all the masses of the particles in the $\tilde{g} \to q\tilde{q} \to \tilde{\chi}_2^0 qq \to \tilde{l}lqq \to \tilde{\chi}_1^0 llqq$ decay chain.

In the focus point region, however, the statistics of lepton pairs is not very high to begin with, and the three-body decays of the gluino and the presence of top quarks in most of these decays result in a large number of jets (between four and twelve, depending on the gluino and top decay modes), which comes from the decay of two gluinos. It is thus very difficult to control the resulting jet combinatorics in these events.

Instead, the strategy used was the explicit reconstruction of a top quark in the event using the hadronic decay mode, followed by the selection of $t\bar{t}$ and $t\bar{b}/\bar{t}b$ pairs, with appropriate kinematic cuts (in particular, the angular separation) in order to reconstruct the $\tilde{g} \to t\bar{t}\tilde{\chi}^0$ and $\tilde{g} \to t\bar{b}\tilde{\chi}^-$ decays. The invariant mass distributions of these decays are shown at the parton level in Fig. 11.

The distribution of the $t\bar{t}$ invariant mass has four endpoints; one for each neutralino state. Because of the poor experimental resolution on the reconstructed momentum of the top, they are unlikely to be separated from the data. The distribution falls almost linearly to the third endpoint at $m(\tilde{g}) - m(\tilde{\chi}_2^0) = 696\,\text{GeV}$, and only very few events due to the $\tilde{g} \to \tilde{\chi}_1^0 t\bar{t}$ decay are found at a larger invariant mass.

The distribution of the $t\bar{b}$ invariant mass has two endpoints at 569.8 GeV and 707.2 GeV, corresponding to the difference between the mass of the gluino and the masses of the two charginos. Again, the first endpoint will be very difficult to extract from the data, because of the smearing from the finite jet energy resolution.

5.1 Reconstruction of the $\tilde{g} \to \tilde{\chi}^0 t\bar{t}$ decay

The reconstruction of the $t\bar{t}$ invariant mass using the decay $t\bar{t} \to jjbjj\bar{b}$ requires the presence of six jets, two of which

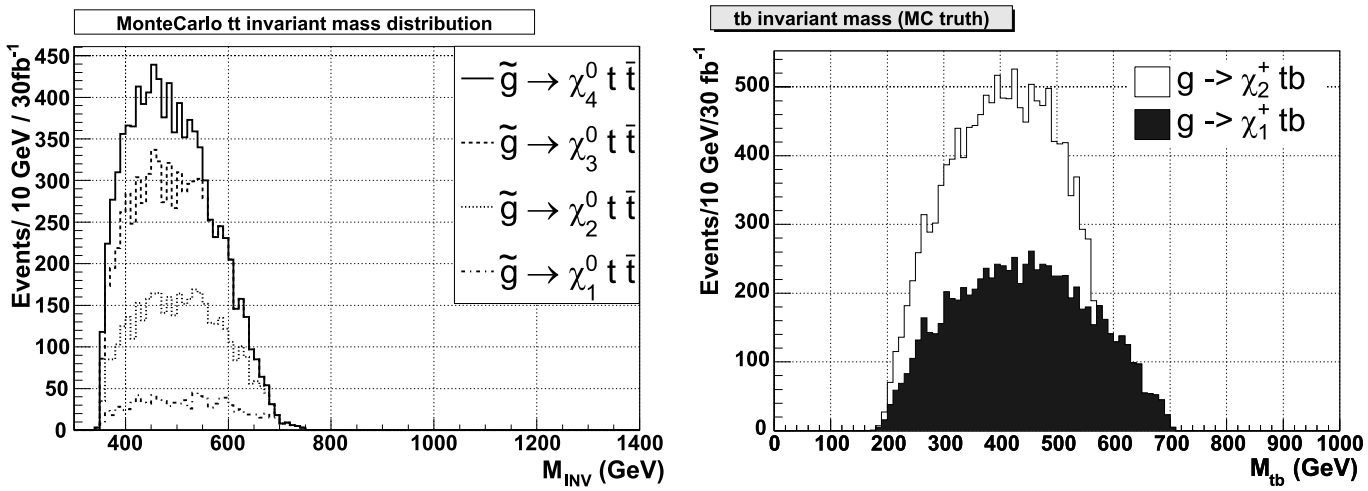

Fig. 11. Parton-level invariant mass of the $t\bar{t}$ pairs from the $\tilde{g} \to tt\tilde{\chi}^0$ decays (*left*) and of the $t\bar{b}$ pairs from the $\tilde{g} \to t\bar{b}\tilde{\chi}^-$ decays (*right*). The contributions from the decay to the various neutralino and chargino states are shown separately

tagged as b-jets to reduce the combinatorial background. Other jets are expected for signal events, from the decay of the other gluino. Thus, events were selected according to following cuts:

- $E_{\mathrm{MISS}}^{\mathrm{T}} > 120$ GeV;
- at least one jet with $p_{\mathrm{T}} > 150$ GeV, at least 8 jets with $p_{\mathrm{T}} > 40$ GeV, and at least two of these tagged as b-jets;
- $M_{\mathrm{EFF}} > 1200$ GeV.

All the pairs of jets that were not b-tagged, with a transverse momentum $p_{\mathrm{T}} > 30$ GeV, and with an invariant mass within ± 20 GeV of the nominal W mass were used to build W candidates. The combinatorial background is estimated from the events that contain jet pairs in the regions **A**: $|m_{jj} - (m_W - 30\,\mathrm{GeV})| < 10$ GeV and **B**: $|m_{jj} - (m_W + 30\,\mathrm{GeV})| < 10$ GeV. We call them the W "sidebands". The energy and momentum of the jet pairs of each sideband are then rescaled linearly by multiplying them by a factor $[m_W + 2(m_{jj} - (m_W \pm 30\,\mathrm{GeV}))]/m_{jj}$, so that their invariant mass lies in the W mass region $m_W \pm 20$ GeV) [32].

Top candidates were found by combining each W candidate with one b-jet with a transverse momentum $p_{\mathrm{T}} > 30$ GeV. The invariant mass of top candidates is shown in Fig. 12. The estimate of the combinatorial background is shown as well. The top mass peak is clearly visible over the background. The top candidates with an invariant mass within ± 20 GeV of the true top mass were selected.

The number of top candidates that pass these selections can be larger than two per event, resulting in a large number of possible top pair combinations. Because of the relativistic boost, the top pairs coming from the decay of one gluino have a smaller average angular separation than the pairs of top coming from the decay of different gluinos or those coming from the standard model $t\bar{t}$ production. In order to reduce the standard model and the SUSY background, the angular separation ΔR (in the (η, ϕ) plane) between the two top candidates was required to be smaller than 2.5. If more than one top pair passes this selection, we select the combination which minimizes

$$\sqrt{(m_{t1} - M_t)^2 + (m_{t2} - M_t)^2}\,, \tag{5}$$

where m_{t1} and m_{t2} are the invariant masses of the two top candidates and M_t is the true top mass.

The number of events that pass the various selections is shown in Table 6 for low-luminosity running conditions and an integrated luminosity of 10 fb^{-1}. The dominant standard model backgrounds after the inclusive cuts on jets, b-jets, missing energy and effective mass (fourth column of Table 6) are the $t\bar{t}$ and the $bb+$jets production. The latter is removed when the reconstruction of the hadronic decay of two top quarks with $\Delta R < 2.5$ is required (last col-

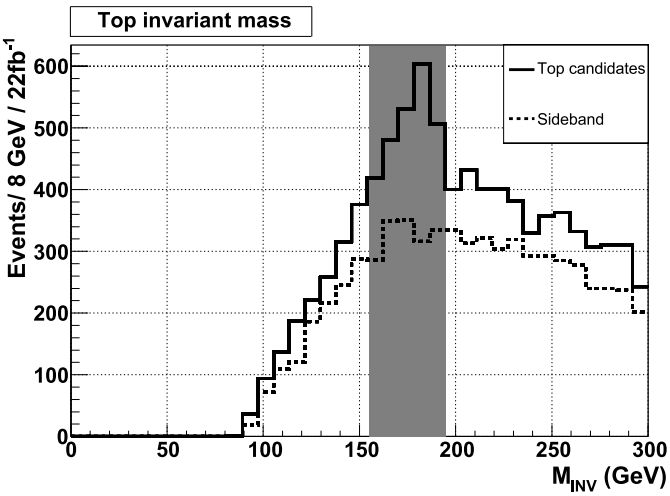

Fig. 12. Distribution of the invariant mass of the top quark candidates (*black line*) and of the combinatorial background estimated from the data, as described in the text (*dashed line*). The plot corresponds to 22 fb^{-1} of low-luminosity data and includes both the supersymmetric signal and the standard model background. The *shaded area* indicates the window used to select good top candidates

Table 6. Efficiency of the cuts used for the reconstruction of the decay of the gluino into $t\bar{t}\tilde{\chi}^0$, evaluated with ATLFAST events for low luminosity operation. The number of events corresponds to an integrated luminosity of 10 fb^{-1}. The third column contains the number of events that pass the cuts on the leading jet, transverse missing energy and effective mass described in the text. The fourth column adds the requirement on the presence of eight jets with $p_{\mathrm{T}} > 40$ GeV, two of which tagged as b-jets. The fifth column reports the number of events with two reconstructed top candidates which satisfy all cuts, except the ΔR cut between the two candidates, which is added to obtain the number of events reported in the last column. SUSY events are divided in those with the presence of the $\tilde{g} \to \tilde{\chi}^0 t\bar{t}$ decay (signal), and those without this decay (background)

Sample	Events	preselection	Eight jets	two top (no ΔR)	two top (final)
SUSY signal	4708	2301	597	80	51
SUSY back.	45 292	311	15	1	1
$t\bar{t}$	7.6×10^6	15 885	397	10.9	3.3
$W+$jets	10.1×10^6	18 279	28	0.5	0.5
$Z+$jets	3.15×10^6	7132	11	0.5	0.5
$bb+$jets	272×10^6	8103	364	0	0

umn of the table), and the dominant background remains the $t\bar{t}$ production, which is however more than one order of magnitude smaller than the signal.

The invariant mass of the top pair is shown in Fig. 13 for low-luminosity running conditions and an integrated luminosity of $10\,\mathrm{fb}^{-1}$. The statistical significance of the excess of events over the standard model contribution is $\mathrm{SUSY}/\sqrt{\mathrm{SM}} = 7.1$ for an integrated luminosity of $1\,\mathrm{fb}^{-1}$, which is comparable with the significance expected from the inclusive search and from the dilepton analysis.

The distribution of the $t\bar{t}$ pair invariant mass for high-luminosity conditions and integrated statistics of $300\,\mathrm{fb}^{-1}$ is shown in Fig. 14. The high luminosity implies a poorer jet resolution and a b-tagging efficiency of 0.5 for the same u-jet mistag probability of 0.01. Only the SUSY

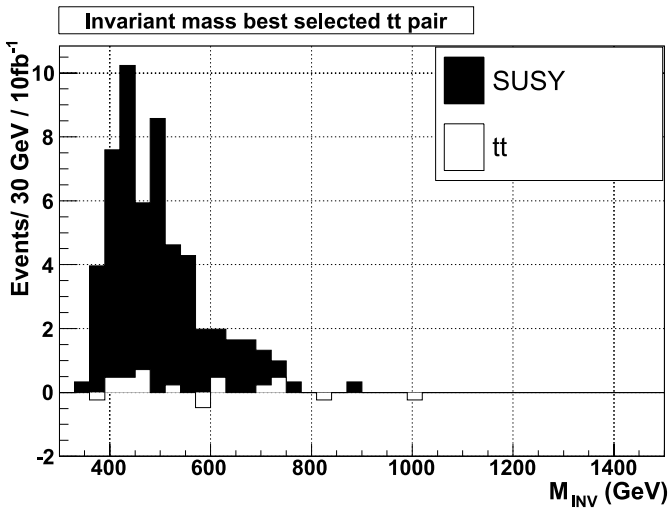

Fig. 13. Distribution of the invariant mass of the selected pairs of reconstructed top quarks. The plot corresponds to $10\,\mathrm{fb}^{-1}$ of low-luminosity data

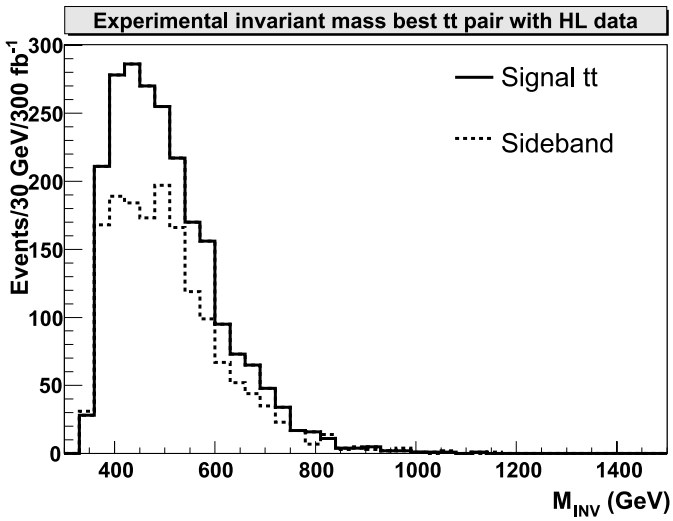

Fig. 14. Distribution of the invariant mass of the selected pairs of reconstructed top quarks. The plot corresponds to $300\,\mathrm{fb}^{-1}$ of high-luminosity data

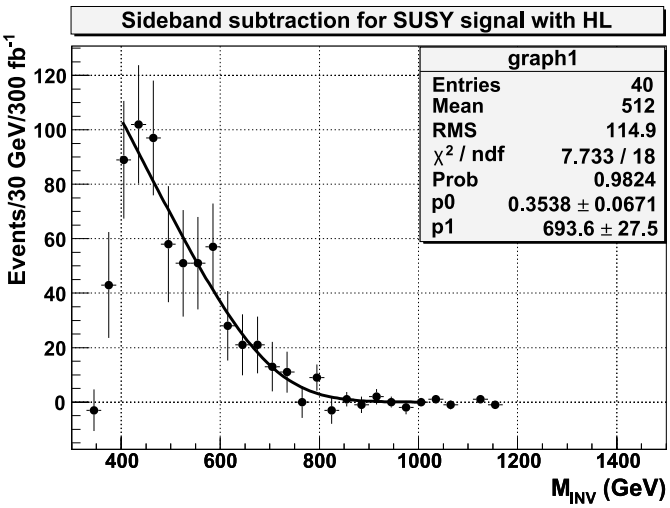

Fig. 15. Distribution of the invariant mass of the selected pairs of reconstructed top quarks, after the subtraction of the background estimated with the side-band technique. The plot corresponds to $300\,\mathrm{fb}^{-1}$ of high luminosity data

contribution is included in the analysis for high luminosity. The contribution from the combinatorial background, estimated with top pairs built using the fake W candidates, is also shown. The distribution obtained after the subtraction of this contribution is drawn in Fig. 15. In order to estimate the position of the endpoint, a fit was performed with a polynomial of first order convoluted with a Gaussian. The Gaussian represents the experimental resolution on the top pair invariant mass and has been set to 15% of the endpoint value. The agreement of this function with the data is excellent. The endpoint is found to be (694 ± 28) GeV, in pretty good agreement with the value of $m(\tilde{g}) - m(\tilde{\chi}_2^0) = 696$ GeV. The interpretation of the endpoint in terms of this specific mass difference relies on the information from the Monte Carlo truth. Still, the endpoint of the distribution of Fig. 15 provides an estimate of the mass difference between the gluino and the neutralino states.

5.2 Reconstruction of the $\tilde{g} \to \tilde{\chi}^- t\bar{b}$ decay

The reconstruction of the $t\bar{b}$ invariant mass using the decay $t\bar{b} \to jjb\bar{b}$ requires the presence of four jets, two of which tagged as b-jets to reduce the combinatorial background. Other jets are expected for signal events, from the decay of the other gluino and/or the chargino. Thus, events were selected according to the following cuts:

- $E_{\mathrm{MISS}}^{\mathrm{T}} > 120$ GeV;
- at least one jet with $p_{\mathrm{T}} > 200$ GeV, at least 6 jets with $p_{\mathrm{T}} > 60$ GeV, and at least two b-jets with $p_{\mathrm{T}} > 30$ GeV;
- $M_{\mathrm{EFF}} > 1200$ GeV.

The top candidates were reconstructed as explained in the previous section. They were also required to have a transverse momentum $p_{\mathrm{T}} > 150$ GeV. If more than one candidate satisfied these selections, the one with the invariant mass closest to the top mass was selected.

Each of the top candidates was combined with the b-jets present in the event. Only the $t\bar{b}$ pairs with an angular separation $\Delta R < 2$ between the top reconstructed direction and the b-jet were considered. In the events where more than one tb pair satisfy these selections, the smallest invariant mass of these pairs should be less than the kinematical endpoint of the signal. Since combinatorial background pairs with an invariant mass larger than the kinematical endpoint of the signal would make the identification of the endpoint difficult, the combination with the smallest invariant mass was selected.

The efficiency of the various cuts is reported in Table 7. For an integrated luminosity of $10\,\mathrm{fb}^{-1}$, 332 SUSY events and 190 standard model events pass all the selection cuts, including those on the reconstructed tb pair. In 241 of the SUSY events the $\tilde{g} \to \tilde{\chi}^- t\bar{b}$ decay is present in the Monte Carlo truth. They are classified as signal in the table, showing the efficiency of the selections for these events.

However, the reconstructed tb pair matches the one from the decay only in 24 of those events. In the other SUSY events the reconstructed top does not have a correspondence in the MC truth (usually because of the incorrect pairing of jets to build the W candidates), or the tb pair matches a true top and bottom quarks originating from a $\tilde{g} \to \tilde{\chi}^0 t\bar{t}$ decay or from the decay of two different gluinos. The SUSY events thus pass the analysis selections with good efficiency, making this channel a promising one for SUSY discovery, but the probability to reconstruct the correct tb pair is relatively small, making it difficult to reconstruct the kinematic endpoint in the invariant mass distribution.

The dominant standard model background is again $t\bar{t}$. The statistical significance $\mathrm{SUSY}/\sqrt{\mathrm{SM}}$ is 7.6 for an integrated luminosity of $1\,\mathrm{fb}^{-1}$; this is comparable to the significance provided by the other searches presented here (inclusive, dilepton and $t\bar{t}$ analysis). The SUSY/SM ratio is smaller, however, than in the leptonic and $t\bar{t}$ analysis, and the standard model contribution to the effective mass distribution cannot be neglected. The distribution of the effective mass of the $t\bar{b}$ pairs is reported in Fig. 16, for an integrated luminosity of $10\,\mathrm{fb}^{-1}$. The events are divided in the following classes.

- SUSY events in which the selected $t\bar{b}$ pair does indeed correspond to the pair coming from the decay $\tilde{g} \to \tilde{\chi}^- t\bar{b}$.
- SUSY events, in which the reconstructed top and b-jet do correspond to top and bottom quarks in the Monte Carlo truth, but these quarks come from the decay $\tilde{g} \to \tilde{\chi}^0 t\bar{t} \to \tilde{\chi}^0 bWbW$. These events have not been classified under "SUSY background", because the invariant mass of the top with the bottom quark coming from the decay of the other top also has four kinematic edges, corresponding to $m(\tilde{g}) - m(\tilde{\chi}^0) - m(W)$.
- SUSY events in which the b-jet or the reconstructed top does not have a correspondence in the MC truth (usually because of the incorrect pairing of jets to build the W candidates) or the corresponding quarks come from the decay chain of two different gluinos. These events are classified as "SUSY background". In many of these events the $\tilde{g} \to \tilde{\chi}^- t\bar{b}$ decay is present in the Monte Carlo truth, and they are thus classified as signal in Table 7, but the reconstructed top and bottom do not match those from the decay. The contribution from the fake top candidates can be estimated from the sideband distribution reported as a dashed line.
- Standard model events.

The contribution from the SUSY and $t\bar{t}$ backgrounds is large, and the statistics near the expected kinematic endpoint is scarce. It is thus not possible to measure the kinematic endpoint.

Assuming that the contribution of the standard model background is reliably estimated, after subtraction of the standard model and combinatorial backgrounds it may be possible to obtain information on the $m(\tilde{g}) - m(\tilde{\chi}^{\pm})$ difference with larger statistics, but further study is required to evaluate this possibility. However, this analysis remains a promising strategy to find evidence of an excess of events over the standard model contribution.

Table 7. Efficiency of the cuts used for the reconstruction of the decay of the gluino into $\tilde{\chi}^- t\bar{b}$, evaluated with ATLFAST events for low luminosity operation. The number of events corresponds to an integrated luminosity of $10\,\mathrm{fb}^{-1}$. The third column contains the number of events which pass the inclusive cuts on jets, b-jets, missing energy and effective mass. The fourth column reports the number of events with an accepted $t\bar{b}$ pair. SUSY events are divided in events with the presence of the $\tilde{g} \to \tilde{\chi}^- t\bar{b}$ decay in the Monte Carlo truth (signal), and without it (background)

Sample	events	inclusive cuts	$t\bar{b}$ pair
SUSY signal	3453	901	241
SUSY background	46 547	313	91
$t\bar{t}$	7.6×10^6	1127	143
W+jets	10.1×10^6	60	5
Z+jets	3.15×10^6	24	1
bb+jets	272×10^6	873	41

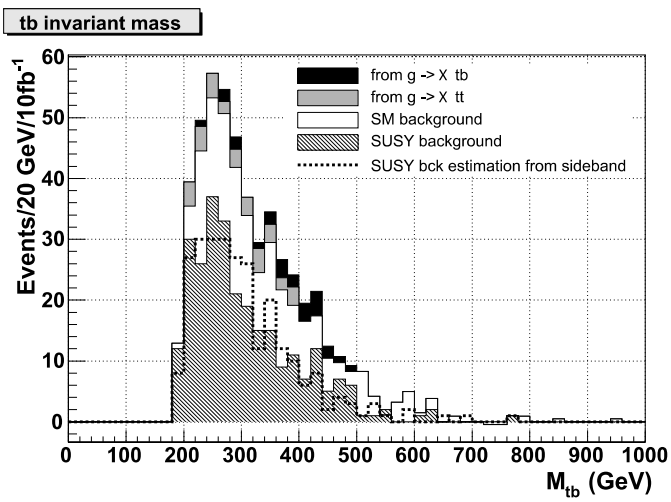

Fig. 16. Distribution of the invariant mass of the selected $t\bar{b}$ pairs. The plot corresponds to $10\,\mathrm{fb}^{-1}$ of low-luminosity data

6 Extraction of the MSSM parameters

In the MSSM, the neutralino and chargino sector of the theory depends on only four parameters: the gaugino masses M_1 and M_2, the higgsino mass term μ, and the ratio between the Higgs vacuum expectation values $\tan\beta$. In many models, including mSUGRA, the gaugino masses are unified at some high scale. This common value is the parameter $m_{1/2}$ in mSUGRA. At the TeV scale the relation

$$M_1 = \frac{5g'^2}{3g^2} M_2 \simeq 0.5 M_2 \tag{6}$$

holds, where g and g' are the electroweak coupling constants. This relation reduces the number of free parameters to three unknowns.

The constraints placed by the dilepton edge analysis on the neutralino mass spectrum can be used to determine the values of M_1, μ and $\tan\beta$ which are compatible with the experimental measurements.

The ISAJET 7.71 code [13] was used to compute the masses and branching ratios of supersymmetric particles as a function of the soft supersymmetry breaking parameters. This provides, in particular, the values of neutralino and chargino masses as a function of M_1, M_2, μ and $\tan\beta$.

For each point of parameter space the mass differences $\Delta M_2 = m(\tilde{\chi}_2^0) - m(\tilde{\chi}_1^0)$ and $\Delta M_3 = m(\tilde{\chi}_3^0) - m(\tilde{\chi}_1^0)$ were compared to the measured values $\Delta M_2^{\rm exp} = 57.2\,\text{GeV}$ and $\Delta M_3^{\rm exp} = 78.1\,\text{GeV}$ obtained using $300\,\text{fb}^{-1}$ of simulated data, as discussed in Sect. 4. The following χ^2 was evaluated:

$$\chi^2 = \left(\Delta M_2 - \Delta M_2^{\rm exp}\right)^2 / \sigma_2^2 + \left(\Delta M_3 - \Delta M_3^{\rm exp}\right)^2 / \sigma_3^2 - 2r \left(\Delta M_2 - \Delta M_2^{\rm exp}\right)\left(\Delta M_3 - \Delta M_3^{\rm exp}\right) / \sigma_2\sigma_3 \,, \tag{7}$$

where $\sigma_2 = 0.4\,\text{GeV}$ and $\sigma_3 = 1.4\,\text{GeV}$ are the errors on the measurements of ΔM_2 and ΔM_3 respectively, and $r = 0.038$ is the correlation coefficient.

The points in the parameter space that have a χ^2 probability larger than 0.05 were selected. In addition, the same sign was required for the $\tilde{\chi}_2^0$ and $\tilde{\chi}_1^0$ mass eigenstates and the opposite sign for the $\tilde{\chi}_3^0$ and $\tilde{\chi}_1^0$ mass eigenstates, since a good fit of the dilepton invariant mass distribution can be obtained only under these hypotheses, as discussed in Sect. 4.

A scan of the values of the parameters M_1, μ and $\tan\beta$ was then performed, using (6) to fix the value of M_2, to find the parameter space that gives masses compatible with the simulated experimental constraints determined in Sect. 4. The scan was performed in the range

$$45\,\text{GeV} < M_1 < 500\,\text{GeV}, \quad 45\,\text{GeV} < |\mu| < 1000\,\text{GeV}, \quad 1 < \tan\beta < 65 \tag{8}$$

in steps of 2 GeV for M_1 and μ, for 16 values of $\tan\beta$, and for both positive and negative values of μ, so that a total of 3×10^6 values in the parameter space were considered. The region in this space that is compatible with the simulated ATLAS constraints is shown in Fig. 17 for positive values of μ and in Fig. 18 for negative values of μ.

The left plot shows the allowed values of M_1 and μ. Each parameter can vary in a relatively large interval: $97\,\text{GeV} < M_1 < 136\,\text{GeV}$ and $138\,\text{GeV} < \mu < 182\,\text{GeV}$ for positive values of μ, $116\,\text{GeV} < M_1 < 157\,\text{GeV}$ and $-208\,\text{GeV} < \mu < -168\,\text{GeV}$ for negative values of μ. However, the ratio is more constrained to the range $1.32 < \mu/M_1 < 1.46$. The value of $\tan\beta$ is not constrained by the experimental data.

The value of the ratio between μ and M_1 is interesting, since in most of mSUGRA space $\mu \gg M_2 \simeq 2M_1$. With this hierarchy between the parameters, the lightest neutralino is almost a pure bino. The focus point region of mSUGRA,

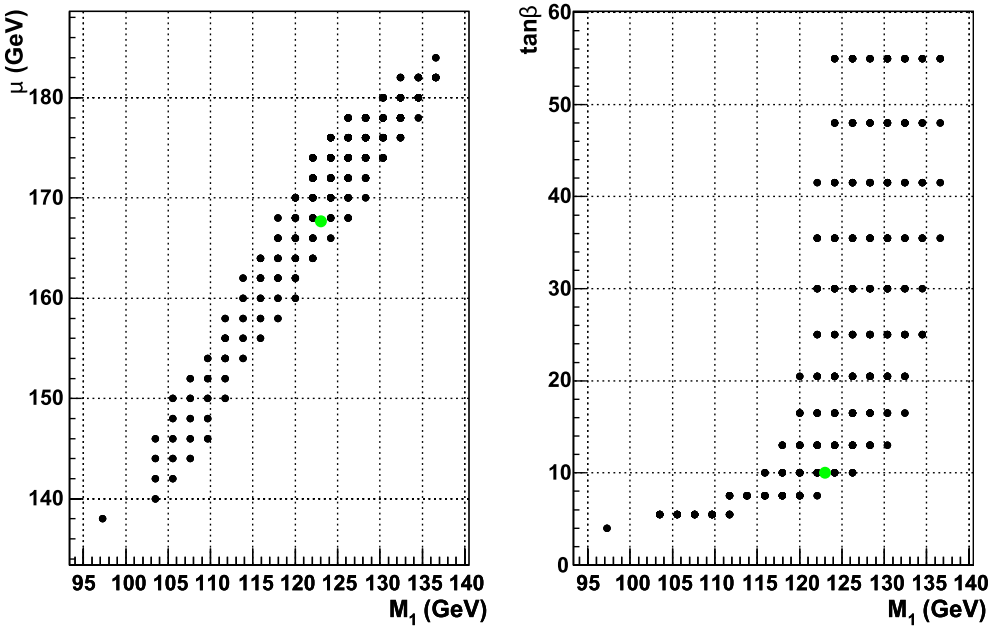

Fig. 17. Values of the MSSM parameters μ, M_1 and $\tan\beta$ that are compatible with the experimental constraints on the neutralino mass spectrum obtained with $300\,\text{fb}^{-1}$ of data and at 95% confidence level, for positive values of μ

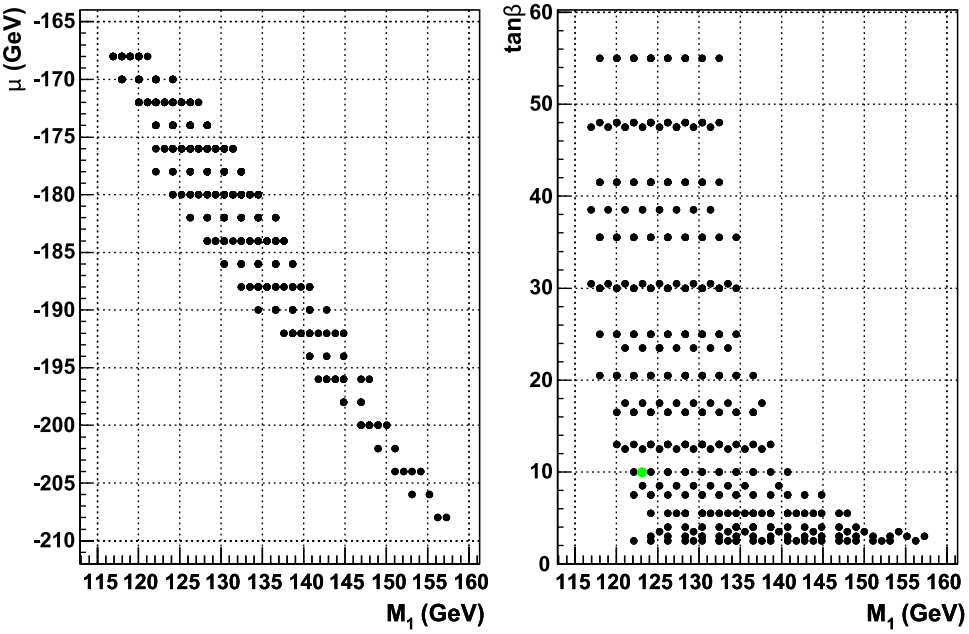

Fig. 18. Values of the MSSM parameters μ, M_1 and $\tan\beta$ that are compatible with the experimental constraints on the neutralino mass spectrum obtained with 300 fb^{-1} of data and at 95% confidence level, for negative values of μ

instead, is characterized by $\mu \simeq M_1$ [8–11]. In this case the mixing between gauge eigenstates is nearly maximal and each mass eigenstate receives a significant contribution from all the gauge eigenstates. The higgsino component of the $\tilde{\chi}_1^0$ allows for rapid s-channel neutralino annihilation, which is the mechanism that reduces the relic density in the early universe. The measurement of the two leptonic edges allows one to establish this scenario.

For any given set of values of the parameters M_1, M_2, μ and $\tan\beta$ the masses of the neutralinos and their gaugino mixing angles can be computed, so these quantities are also constrained by the data. For the values of the parameters that are compatible with the dilepton invariant mass data at 95% C.L. the mass of the lightest neutralino lies in the range $67\,\text{GeV} < m(\tilde{\chi}_1^0) < 156\,\text{GeV}$. For any given value of the mass of $\tilde{\chi}_1^0$, the masses of the next two lightest neutralinos are precisely constrained from the measurements of the two edges of the dilepton distribution.

7 Conclusions

A study of the potential of ATLAS of detecting and measuring supersymmetry in the focus point scenario has been presented. For the selected point in the parameter space the observation of an excess of events over the standard model expectations should be observed rather easily; the time needed for discovery would probably be determined by the understanding of the systematics related to the detector response and knowledge of the standard model backgrounds rather than the statistical significance. Several channels can contribute to the discovery of an excess of SUSY events with a comparable statistical significance: with appropriate kinematic cuts, the presence of supersymmetry physics may become manifest through an excess of events with hard jets, large missing energy and b-jets (Sect. 3), events with hard jets, large missing energy and opposite-sign electron or muon pairs (Sect. 4), and events with hard jets, large missing energy, a top and a bottom quark or two top quarks (Sect. 5). In each of these channels, the contribution from SUSY events has a statistical significance between 6.1 and 8.2 standard deviations with 1 fb^{-1} of data.

In the focus point region, the neutralino leptonic decays proceed through a direct three-body decay in which the virtual slepton exchange is negligible, because of the large scalar mass. An analytical expression was derived in Sect. 4 for the distribution of the invariant mass of the resulting lepton pairs. This formula was used to fit the distribution of opposite-sign lepton pairs obtained with 300 fb^{-1} of simulated LHC data. Two kinematic edges, measuring the $m(\tilde{\chi}_3^0) - m(\tilde{\chi}_1^0)$ and $m(\tilde{\chi}_2^0) - m(\tilde{\chi}_1^0)$ mass differences, are measured with a precision of the order of 1 GeV.

The constraints that this measurement would place on the MSSM gaugino sector parameters have been discussed. These constraints are such that a scenario with a large mixing in the neutralino sector and a relic neutralino density of the same order of magnitude as the dark matter abundance would emerge from the LHC measurements.

The gluino decay into $t\bar{t}\tilde{\chi}^0$ and $t\bar{b}\tilde{\chi}^+$ can be studied through the reconstruction of the tt and $t\bar{b}$ invariant mass. While a precise reconstruction of the corresponding kinematic edges does not seem to be possible, evidence for these decays and an estimate of the mass difference between the gluino and gaugino states may be extracted from the experimental data.

Acknowledgements. The authors wish to thank G. Polesello (Pavia) and F. Ragusa (University of Milano) for their helpful suggestions on the analysis and on the preparation of this document. They also thank D. Tovey (Sheffield), F. Paige (BNL) and I. Hinchliffe (LBNL), as well as M.M. Nojiri (KEK, Tsukuba), for useful discussions and advices.

The authors are also grateful to S. Asai and the colleagues of the University of Tokyo for providing the ALPGEN 4-vector files used in the production of the $W+$jets and $Z+$jets backgrounds, and to B. Gjelsten (Bern) for the production of the $Z+$jets fast simulation ntuples.

This work has been performed within the ATLAS collaboration making use of the detector fast simulation and tools, which are the result of collaboration-wide efforts.

References

1. H.P. Nilles, Phys. Rev. **110**, 1 (1984) and references therein
2. LEP (ALEPH + DELPHI + L3 + OPAL experiments) SUSY working group page, http://lepsusy.web.cern.ch/lepsusy, and references therein
3. D.N. Spergel et al., astro-ph/0603449
4. C.L. Bennett et al., Astrophys. J. Suppl. **148**, 1 (2003)
5. D.N. Spergel et al., Astrophys. J. Suppl. **148**, 175 (2003)
6. J.R. Ellis et al., Phys. Lett. B **565**, 176 (2003)
7. H.W. Baer, C. Balazs, J. Cosmol. Astropart. Phys. **0305**, 006 (2003)
8. J.L. Feng, K.T. Matchev, T. Moroi, Phys. Rev. Lett. **84**, 2322 (2000) [hep-ph/9908309]
9. J.L. Feng, K.T. Matchev, T. Moroi, Phys. Rev. D **61**, 075 005 (2000) [hep-ph/9909334]
10. J.L. Feng, K.T. Matchev, F. Wilczek, Phys. Lett. B **482**, 388 (2000) [hep-ph/0004043]
11. J.L. Feng, K.T. Matchev, F. Wilczek, Phys. Rev. D **63**, 045 024 (2001) [hep-ph/0008115]
12. G.B. Belanger, F. Boudjema, A. Pukhov, A. Semenov, Comput. Phys. Commun. **174**, 577 (2006) [hep-ph/0405253]
13. H. Baer, F.E. Paige, S.D. Prototopescu, X. Tata, hep-ph/0312045
14. B.C. Allanach, Comput. Phys. Commun. **143**, 305 (2002) [hep-ph/0104145]
15. B.C. Allanach et al., JHEP **0303**, 016 (2003) [hep-ph/0302102] and references therein
16. B.C. Allanach et al., hep-ph/0402161
17. G. Belanger, S. Kraml, A. Pukhov, Phys. Rev. D **72**, 015 003 (2005) [hep-ph/0502079]
18. ATLAS Physics Performance and Detector Technical Design Report, CERN/LHCC 99-14 (1999)
19. Tevatron Electroweak Working Group, hep-ex/0608032
20. G. Corcella et al., JHEP **0101**, 010 (2001)
21. S. Moretti et al., JHEP **0204**, 028 (2002)
22. G. Corcella et al., hep-ph/02010213
23. S. Frixione, B.R. Webber, JHEP **0206**, 029 (2002) [hep-ph/0204244]
24. S. Frixione, P. Nason, B.R. Webber, JHEP **0308**, 007 (2003) [hep-ph/0305252]
25. M.L. Mangano, M. Moretti, F. Piccinini, R. Pittau, A. Polosa, JHEP **0307**, 001 (2003) [hep-ph/0206293]
26. M.L. Mangano, M. Moretti, R. Pittau, Nucl. Phys. B **632**, 343 (2002) [hep-ph/0108069]
27. F. Caravaglios, M.L. Mangano, M. Moretti, R. Pittau, Nucl. Phys. B **539**, 215 (1999) [hep-ph/9807570]
28. E. Richter-Was, D. Froidevaux, L. Poggioli, ATL-PHYS-96-079 and ATL-PHYS-98-131
29. ATLAS High-Level Trigger, Data Acquisition and Controls Technical Design Report, CERN/LHCC 2003-022 (2003)
30. M.M. Nojiri, Y. Yamada, Phys. Rev. D **60**, 015 006 (1999)
31. S. Montesano, Ricerca di Particelle Supersimmetriche nell'ambito dell'esperimento ATLAS, Diploma Thesis (University of Milano, 2006)
32. J. Hisano, K. Kawagoe, M. Nojiri, Phys. Rev. D **68**, 035 007 (2003)
33. C.K. Gjelsten et al., ATL-PHYS-2004-007
34. C.K. Gjelsten et al., JHEP **12**, 003 (2004)